Materials Horizons

ROYAL SOCIETY OF CHEMISTRY

COMMUNICATION

View Article Online
View Journal | View Issue

Cite this: *Mater. Horiz.*, 2023, **10**, 2487

Received 15th March 2023,
Accepted 26th March 2023

DOI: 10.1039/d3mh00391d

rsc.li/materials-horizons

Selective spectral absorption of nanofibers for color-preserving daytime radiative cooling†

Xiangshun Li,[a] Huilin Xu,[a] Yuchen Yang,[a] Faxue Li,[a] Seeram Ramakrishna,[b] Jianyong Yu,[c] Dongxiao Ji *[a] and Xiaohong Qin *[a]

Passive radiative cooling is a promising solution for cooling objects without consuming energy. However, chemical colors absorb visible light and generate heat, posing a challenge in the design of a colored sub-ambient daytime radiative cooler (CSDRC) in a simple and scalable way. Herein, we used nanofibers (NF) to achieve selective spectral absorption of the daytime radiative cooler through a dope-dyeing electrospinning technique. This approach allows for the selective absorption of desired colors in the visible spectrum, while the nanofiber structure provides strong visible and near-infrared light scattering to minimize solar heating. We selected cellulose acetate (CA) with mid-infrared emittance characteristics for efficient sky cooling. Our design enabled the CA NF CSDRC to exhibit an ultra-high NIR reflectance of 99%, a high MIR emittance of 95%, and vibrant colors. These unique optical properties resulted in a reduction of the maximum ambient temperature by 3.2 °C and a cooling power of ≈40 W m^{-2} at a solar intensity of 700 W m^{-2}. Additionally, the flexibility and deformability of the colored nanofiber cooler make it suitable for thermal management in various practical applications. Our work provides a simple and scalable solution for designing colored passive radiative cooling materials.

New concepts

Passive daytime subambient radiative cooling has the potential to provide sustainable thermal management without consuming external energy. However, the traditional white appearance of radiative coolers may not be aesthetically pleasing in practical situations. This is where a colored sub-ambient daytime radiative cooler (CSDRC) can offer a simple and scalable solution. The challenge, however, is that chemical colors absorb visible light and generate heat, which interferes with the cooling effect. In this study, we demonstrate a novel approach of fabricating a CSDRC using a simple dope-dyeing electrospinning method to create a colored cellulose acetate (CA) nanofiber membrane. Our design achieved a 3.2 °C subambient daytime cooling effect while displaying vibrant colors simultaneously. The CA nanofiber CSDRC also offers excellent flexibility and deformability, making it suitable for various practical applications, such as cooling covers for buildings and textiles. Our work provides a promising solution for designing colored passive radiative cooling materials that can enhance both functionality and aesthetics.

Introduction

Cooling systems account for around 15% of global electricity use,[1] and traditional cooling methods consume enormous amounts of energy and contribute to the greenhouse effect.[2] Passive radiative cooling, which allows objects to emit infrared heat to outer space through the atmospheric transparent window without any energy input, has attracted increasing attention.[3–10] However, in the daytime, radiative cooling needs to mitigate the effects of solar radiation, which is significantly greater than the cooling potential.[11,12] Therefore, an ideal daytime passive radiative cooler requires high solar reflectance and good mid-infrared emittance.[13–16] Recent studies have investigated approaches using spectrally selective surfaces that minimize solar absorption while maximizing emission at mid-infrared wavelengths.[17–22] However, these specialized photonic structures are expensive and may not be easy to access.

Compared to the fabrication of complex photonic structures, designing at the molecular level based on polymer chemical bonding provides a more convenient and scalable pathway to achieve modulation of the IR properties, thereby realizing high cooling efficiency. Among various polymers, cellulose acetate (CA) is expected to have abundant chemical bonds such as C–O and C–O–C, which present a desirable IR emittance in the wavelength band that overlaps with the atmospheric transparency window (8–13 μm).[23,24] As a result, good dissipation of IR heat can be achieved.

[a] *Key Laboratory of Textile Science & Technology, Ministry Education, College of Textiles, Donghua University, 2999 North Renmin Road, Songjiang, Shanghai, 201620, China. E-mail: jidongxiao@dhu.edu.cn, xhqin@dhu.edu.cn*
[b] *Department of Mechanical Engineering, National University of Singapore, Singapore 119260, Singapore*
[c] *Innovation Center for Textile Science and Technology, Donghua University, Shanghai 201620, China*

† Electronic supplementary information (ESI) available. See DOI: https://doi.org/10.1039/d3mh00391d

Strong reflections of the solar spectrum (0.3–2.5 μm) are also required to achieve high-performance daytime radiative cooling. However, typical CA films fabricated by drop-casting are transparent (Fig. S1, ESI†) and cannot meet the demand for high solar reflectance. To address this issue, nanostructures can be designed using Mie theory with similar wavelengths to solar radiation to achieve effective solar radiation reflection.[25–31] However, these radiative coolers usually appear white in color due to strong light scattering, which does not meet aesthetic demands and can cause a glare effect that damages human eyes. To overcome this challenge, a new approach is needed to achieve high solar reflectance while maintaining a visually pleasing appearance.[32,33]

Displaying color through the use of pigments or dyes typically involves absorbing visible (VIS) light that complements the desired color, which inevitably results in heat generation.[25,34] Previous research indicates that near-infrared (NIR) light (780–2500 nm) accounts for 52% of the total solar radiation energy,[32,33] making the improvement of the NIR reflectance of materials the most effective way to reduce solar heating while introducing color into passive radiative cooling materials (Fig. 1a).[35–39]

Combining the molecular and nanoscale structure designs mentioned above, we propose a simple approach to fabricate a chromatic hierarchically structured cellulose acetate (CA) nanofiber (NF) film as a flexible colored sub-ambient daytime radiative cooler (CSDRC) using a dope dyeing electrospinning technique. As a proof of concept, the resulting yellow CA NF film exhibits desirable properties for daytime radiative cooling, with a mid-infrared (MIR) emittance of 95% in the wavelength range of 8–13 μm, an ultra-high near-infrared (NIR) reflectance of 99%, and selective absorption of visible (VIS) light to display the desired color (Fig. 1b). This unique optical property allows the yellow CA NF film to achieve a temperature reduction of up to 3.2 °C compared to ambient temperature at a solar intensity of 700 W m^{-2} and a net radiative cooling power of approximately 40 W m^{-2} at the same solar intensity. Additionally, the CA NF CSDRC possesses excellent flexibility and deformability, making it suitable for various practical applications, including cooling covers for buildings and cooling textiles.

We prepared the CA NF CSDRC through a scalable electrospinning technique (Fig. 2a). The prepared CA NF CSDRCs with assorted colors are displayed in Fig. 2b. The colors demonstrated from left to right are orange, pink, yellow, and blue. The orange color is due to the Fe_2O_3 pigment, while the pink, yellow, and blue colors are endowed by reactive dyestuffs which are commonly used in the textile industry. These dyes and pigments are mixed with CA powder and directly dissolved into the spinning solution to achieve dope-dyeing, and thus no subsequent dyeing process is required. This dyeing process is very simple and therefore has the potential for industrialization. Moreover, the

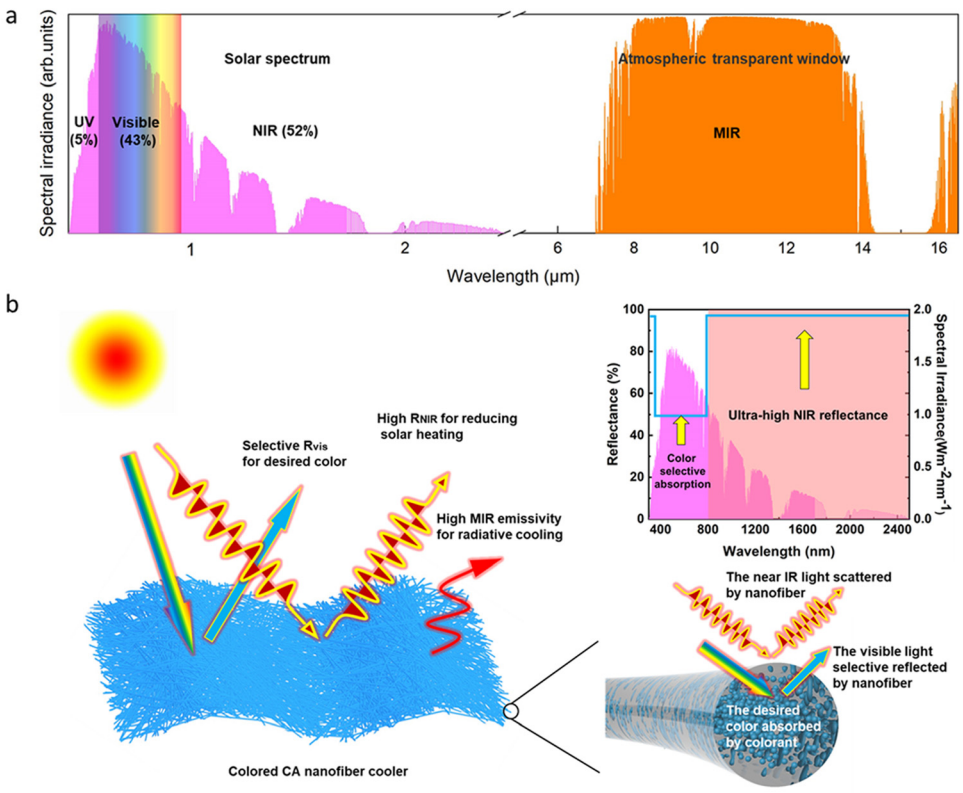

Fig. 1 (a) Spectra of solar spectrum (plotted by AM 1.5G, global tilt) and atmosphere transparent windows. (b) Schematic illustrating the interaction between sunlight and thermal radiation with the CSDRC, which maintains high NIR reflectance while absorbing the specific VIS light to yield the desired color, and high IR heat transfer efficiency, maximizing radiative cooling. A reference of AM 1.5 solar irradiance spectra indicates selective color absorption in the VIS spectrum while enhancing reflectance in the NIR.

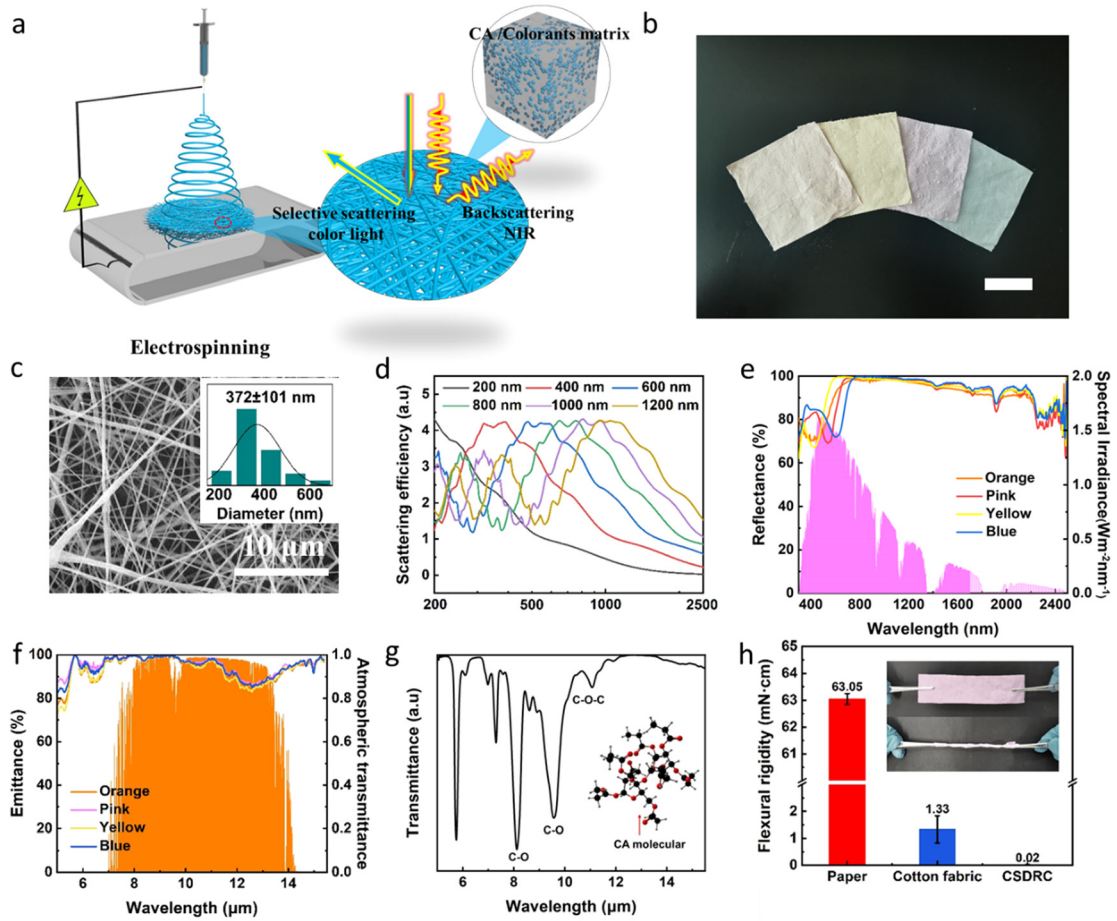

Fig. 2 (a) Schematic illustration of the preparation of CA NF CSDRC. (b) Photograph of CA NF CSDRCs with different colors. The thickness of the film is 500 μm. Scale bar, 5 cm. (c) SEM images of CSDRCs with different colors, insets: the diameter distribution of the corresponding image. (d) The calculated scattering efficiency of CA NF in the solar region. (e) The optical reflectance of CA NF CSDRCs in the solar region. AM1.5 solar spectrum was depicted as a reference. (f) Optical emittance of the CA NF CSDRCs in the MIR region. Atmospheric transmittance was acquired by simulation (Modtran) and depicted as a reference. (g) The IR transmittance of the CA NF CSDRCs in the MIR region. (h) The flexural rigidity comparison of printing paper, cotton fabric and CA NF CSDRC, inset shows the twisted flexible film.

CA NF CSDRC prepared by electrospinning technology has a multilayer disorderly stacked nanofiber structure, which can strongly scatter sunlight and effectively resist external solar heating. We further calculated the scattering efficiency using Mie theory, proving that the diameter size broadly distributed (372 ± 101 nm; Fig. 2c) of CA nanofibers could strongly scatter ultraviolet to near-infrared light across the solar spectrum (Fig. 2d).

These CSDRCs are engineered to be spectrally selective. In the VIS wavelength range (380–780 nm), only VIS wavelengths complementary to the desired color can be absorbed. The spectra of films in the four primary colors reveal the different dominant reflection wavelengths around 401 nm, 540 nm, 446 nm and 620 nm, matching the colors of orange, pink, yellow and blue, respectively (Fig. 2e). The color characteristic of CA NF CSDRC is described numerically by three parameters L, a and b, where 'L' represents the lightness (0 for black, 100 for white).[40,41] Due to the strong scattering effect on VIS light, the L values range of CA NF CSDRCs are between 88–94, indicating these colors are bright. a* represents redness (+)/greenness (−), and b* represents yellowness (+)/blueness (−). The combination of 'a' and 'b' determines color chromaticity. NF CSDRC with different colors possesses varying combinations of 'a' and 'b' (Table S1, ESI†). To intuitively manifest these colors, we also mark such different color coordinate values of NF CSDRC in the commonly used and perceptually uniform CIE (1931) color space. The corresponding points represent color observed with the naked eye, indicating that CA NF CSDRC has enough large color regions for color display (Fig. S2, ESI†). Certainly, these color characteristics are decided by VIS light selective absorption of CA NF CSDRC. In addition to the color, the VIS light selective absorption also affects the cooling capability. The more the VIS light absorption, the color position is far away from the color centers, enabling higher purity colors, but it is also less conducive to cooling. To ensure achieving the sub-ambient cooling effect, the solar-weighted reflectivity of the CA NF cooler is required to reach more than 90%.[19,22] Therefore, it is necessary to balance color and cooling performance by adjusting the amount of selective VIS light absorption.

In the NIR wavelength range (780–2500 nm), the CSDRC is designed to be highly reflective. Owing to the Mie scattering

effect of nanofibers, the optimized NF CSDRCs exhibit ultra-high reflectance of 99% in the NIR wavelengths (Table S2, ESI†). In contrast, the colored CA coating film with the same color shows low NIR reflectance of ≈11% (Fig. S3, ESI†). By changing the concentrations of the pigments and dyes, the shades of the colored nanofiber films can be adjusted, and they still exhibit a high reflectance (above 90%) in the NIR wavelength range (Fig. S4, ESI†). In the MIR wavelength range (8–13 μm), the designed CA NF CSDRCs display a broadband mid-infrared emittance of 95% at the atmospheric transparent window. This broadband mid-infrared emittance is ideal for cooling (Fig. 2f). The strong infrared emission in the 8–13 μm region is mainly attributed to the multiple chemical bonds of C–O and C–O–C of CA molecules providing a strong mid-infrared emission at the atmospheric transparent window (Fig. 2g). In addition, the relevant bonding of C–O stretching, C–N stretching, aromatic C–H bending, and S═O stretching of dyes also contributes to a high emittance in the mid-infrared bands (Fig. S5, ESI†).[42–46]

Moreover, the prepared NF CSDRCs possess excellent flexibility and deformability. As presented in Fig. 2h, the flexural rigidity value (0.02 mN cm) of the pink nanofiber membrane is two orders of magnitude lower than that of the printing paper (63.05 mN cm) and the cotton fabric (1.33 mN cm), demonstrating superior flexibility. And the embedded graphic representation in Fig. 2h shows that the pink nanofiber membrane can be repeatedly stretched and twisted, suggesting its excellent deformability. The good flexibility and deformability enable them to be applied in practical scenarios.

We performed continuous radiative cooling measurements of the CA NF CSDRC on a sunny day in Shanghai, China (120°52′–122°12′E, 30°40′–31°53′N). The outdoor experimental apparatus we used is shown in Fig. 3a and b. To reduce the effect of non-radiative heat exchange consisting of heat conduction and convection on temperature reduction in sub-ambient scenarios, the sample with a thermocouple is placed on an expandable polyethylene foam and then placed inside an acrylic box and covered with a MIR-transparent polyethylene windshield, similar to the experimental setup reported previously.[47,48] A thermometer monitors the surface temperature of the samples and the outside ambient temperature, a solar radiation meter measures the solar intensity in real-time and a hygrometer is used to record the ambient humidity. It is noted that low humidity is conducive to improving the transparency of the atmospheric

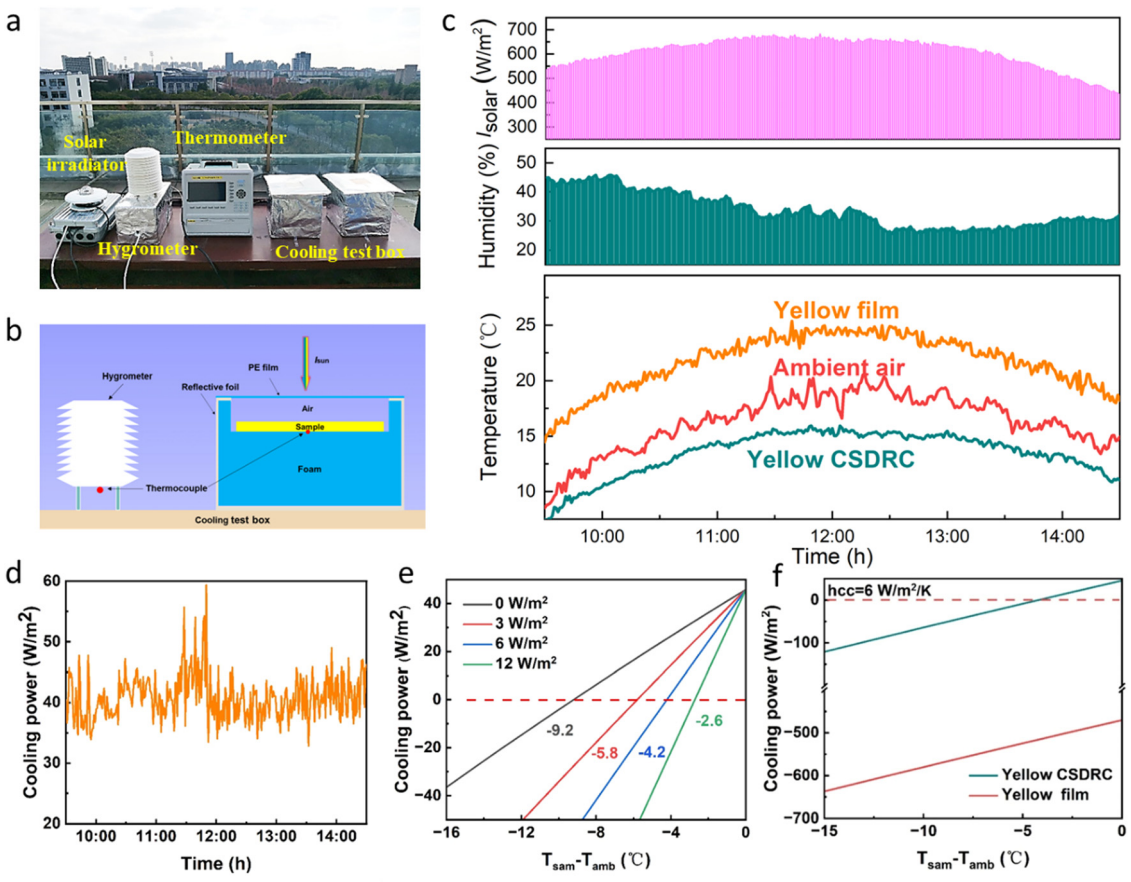

Fig. 3 (a) Picture of the outdoor thermal measurement setup. (b) Schematic of the cooling test box. (c) Real-time monitoring temperature curve of the yellow CSDRC and yellow film (Nov. 2022, Shanghai). (d) Continuous measurement of the radiative cooling power of the yellow CSDRC during the midday. (e) Calculated net cooling power of yellow CSDRC. The variable h_{cc} is a combined nonradiative heat coefficient (h_{cc} is 0, 3, 6, 12 W m^{-2} K^{-1}). (f) The comparison of cooling power of yellow CSDRC and yellow film (h_{cc} = 6 W m^{-2} K^{-1}).

window, thus enhancing the radiative cooling effect of CA NF CSDRC. From 10 : 00 to 14 : 00, under intense solar irradiance of $\sim$700 W m^{-2} and relative humidity of $\sim$30% at noon, the real-time temperature tracking of the air and CA NF CSDRC and CA film are shown in Fig. 3c, the yellow CSDRC shows on average a temperature approximately 3.2 °C below the ambient air temperature, whereas CA film is hotter than the ambient all of the time. In addition, other colors of CA NF CSDRC also exhibit excellent cooling performance compared with the same colors of coating film (Fig. S6, ESI†), which can achieve the cooling effect of 1.6–2.9 °C below the ambient temperature. The results indicate that CA NF CSDRC can achieve a subambient cooling effect by inhibiting solar radiation heating by reflecting the light of other solar bands (especially NIR light) and dissipating the heat to outer space through the infrared high emission characteristics, while the coating film cannot resist the over-incident solar radiation, resulting in the heating effect. The cooling test display that the superior cooling performance of CA NF CSDRC surpasses most of the reported colored daytime radiative coolers (Fig. S7, ESI†).

To estimate the cooling performance of our samples, we use a feedback-controlled heating system to measure the radiative cooling power of the sample. This feedback-controlled heating system maintains the surface temperature of the film at the ambient temperature, and the net cooling power of the sample is equal to the heating power obtained during the testing process. The yellow CSDRC attains an average cooling power of $\approx$40 W m^{-2} under the solar intensity of 700 W m^{-2} during the test process (Fig. 3d). The net cooling power of other CA NF CSDRCs is 10–30 W m^{-2} under the respective test conditions (Fig. S6, ESI†). Fig. 3e presents the net cooling power during the daytime calculated using the radiative cooling theoretical model (see Note S1, ESI†). We set the power of solar radiation to 700 W m^{-2} and different h_{cc} values of 0, 3, 6 and 12 W m^{-2}. The theoretical daytime radiative cooling power of yellow CSDRC can achieve $\approx$45 W m^{-2}, which is close to the measured daytime cooling power but exist certain errors due to the fluctuations in the ambient conditions, the uncertainty in the measurements and the theoretical model approximations. In the ideal limit of no convection and conduction losses (h_{cc} = 0 W m^{-2}), the yellow CSDRC achieves the highest 9.2 °C temperature drop in the daytime temperature, suggesting that the ultra-high NIR reflectance and MIR emittance endows CA NF CSDRCs with high cooling potential. In comparison, the yellow coating film displays $-$472 W m^{-2} of cooling power, revealing the yellow coating film not only has no cooling effect but even produces a heating effect (Fig. 3f). On the other hand, due to the difference in radiative heat load absorption in the visible spectrum, other CA NF CSDRCs also show various cooling power from 15–35 W m^{-2} (from blue to orange) under the same non-radiative heat losses of h_{cc} = 6 W m^{-2} (Fig. S8, ESI†).

In practical applications, the durable stability of cooling capability is significant for the radiative cooler. Here, we further performed a series of experiments to evaluate the durable radiative cooling performance of our CA NF CSDRC. The cooling box with the CA NF CSDRCs is placed outdoor environment for a month, and test their cooling performance

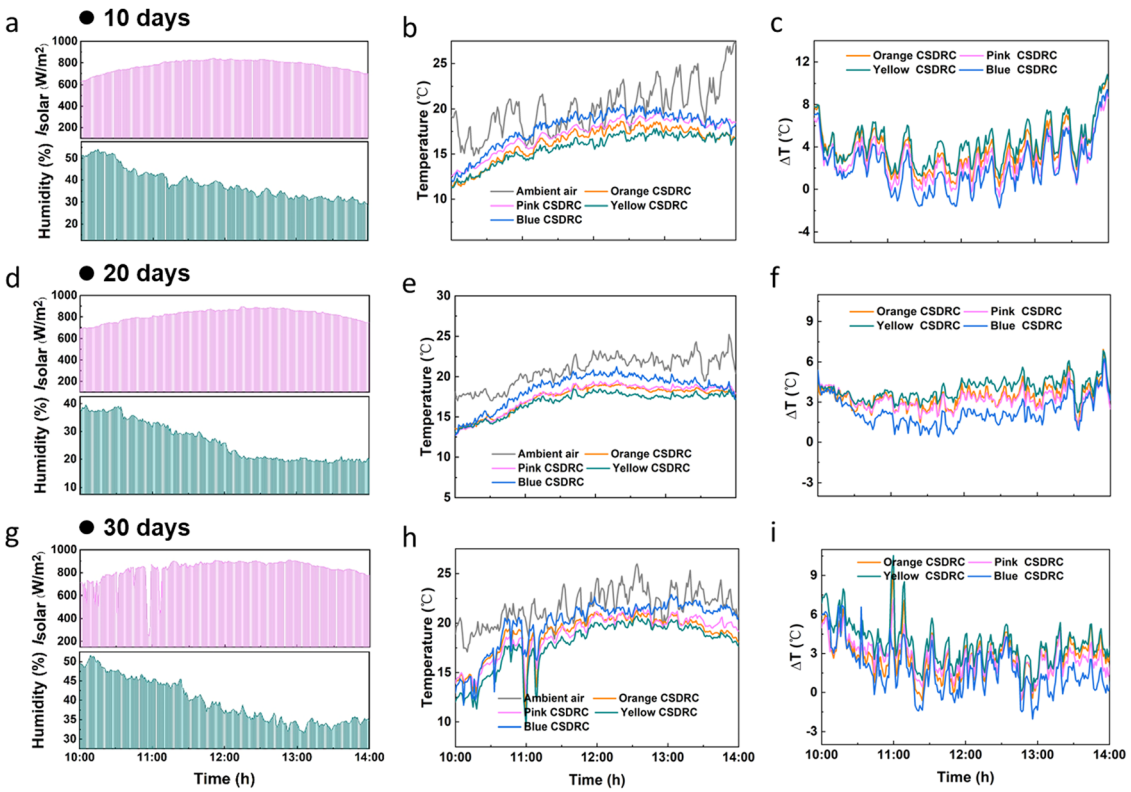

Fig. 4 The cooling stability of the CA NF CSDRC after (a–c) 10 days (d–f) 20 days and (g–i) 30 days of outdoor exposure (In Feb and Mar. 2023).

on days 10, 20 and 30 respectively. As shown in Fig. 4a–c, after 10 days, under clear skies with ~800 W m^{-2} solar intensity and humidity conditions ~30%, the CA NF CSDRC can cool up to 2.1–4.3 °C (from blue to yellow) lower than the ambient temperature. As time increased up, the CA NF CSDRC still displays stable daytime cooling behavior. At day 20, the CA NF CSDRC can achieve 2.0–3.8 °C subambient cooling effect (Fig. 4d–f). After 30 days of exposure in an outdoor environment, we found that the surface temperature of CA NF CSDRC can still cool up to 1.6–3.7 °C lower than the ambient temperature, indicating their superior cooling stability (Fig. 4g–i). Additionally, we also investigate the spectral stability of the CA NF CSDRC. After 30 days of the outdoor placement, the color depth of the CSDRC is slightly reduced because the chromogenic system of a part of dye molecule is damaged due to absorption of solar light energy, resulting in slight fading of dye (Fig. S9a and b, ESI†); however, it also means that CSDRC can reduce VIS absorption and increase VIS reflectance, thus having a positive effect on the cooling (Fig. S9c–f, ESI†). In summary, the CA NF CSDRC possesses excellent durable stability in esthetic and continuous cooling properties.

Practically, CA NF CSDRCs can be widely applied in various energy-saving thermal management systems, such as cooling systems for buildings, vehicles, and even our bodies. Utilizing the excellent flexibility, deformability and passive radiative cooling capacity of the NF CSDRC, we have demonstrated various potential applications in daily activities. For instance, the CA NF CSDRC can be applied to the garment. As displayed in Fig. 5a, due to the superior flexibility, the NF CSDRC adheres well to the skin like regular cotton fabrics. Not only that, under the ~500 W m^{-2} of solar radiation, the CA NF CSDRC shows a better cooling effect compared to summer clothes, which drop the temperature to about 2.3 °C (Fig. 5b), displaying immense potential in the wearable market. Next, we exhibit the case utilizing CA NF CSDRC on the vehicle cooling (Fig. 5c). Since the sun heats the vehicle exposed to the outdoors, the temperature of the cab can rise sharply and even lead to safety accidents. Thus, we fitted the CA NF CSDRC onto a car model, recorded the temperature for 30 min under direct sunlight, and compared it to the case without the CSDRC. A maximum temperature drop of 6 °C is observed for the covered device under the ~900 W m^{-2} of solar radiation (Fig. 5d). In another example, as shown in (Fig. 5e), the tent is decorated with a CA NF CSDRC and conventional fabric (the same color with CA NF SCDRC, Fig. S10, ESI†), respectively and is placed on the lawn and exposed to the sunlight. Through tracking the temperature inside the tent, and the results show that the ordinary tent achieved a higher average temperature. Compared to the

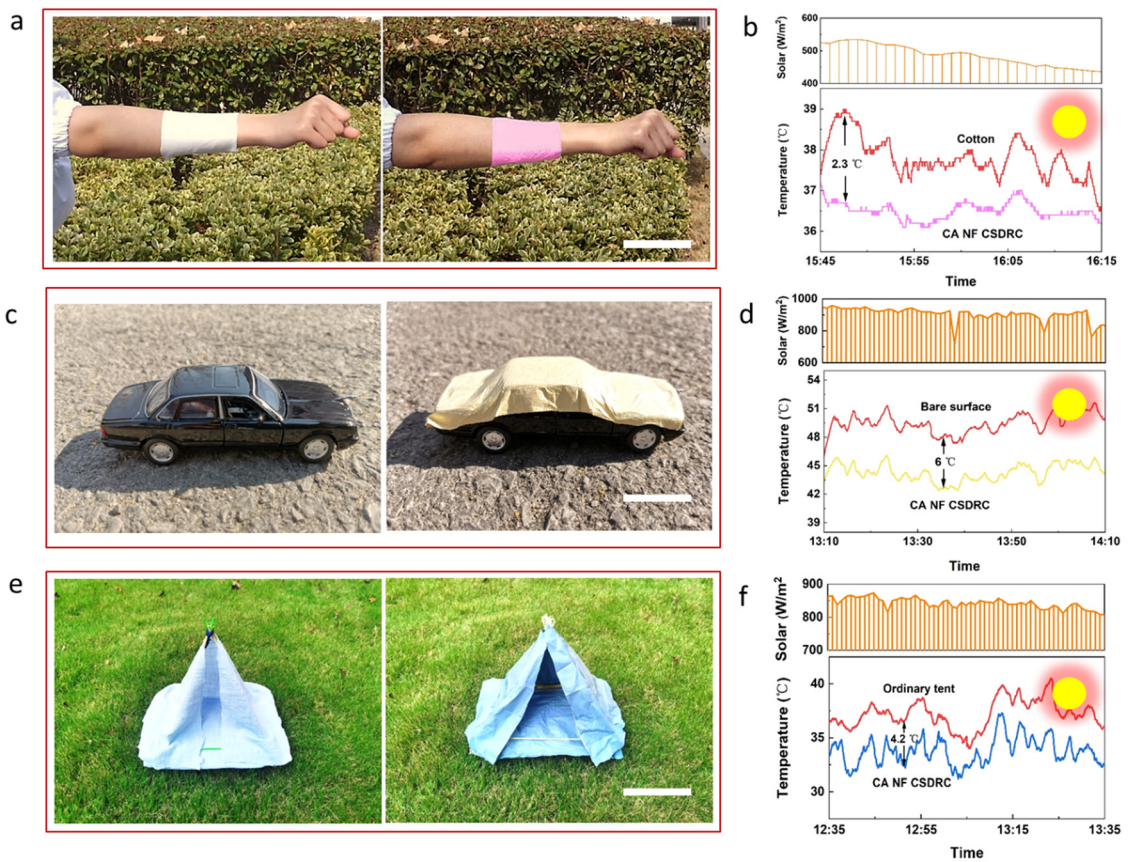

Fig. 5 (a) The photo and (b) the comparison of the cooling effect of white cotton fabric and NF CSDRC. Scale bar, 10 cm. The (c) photo and (d) temperature tracking for a car covered and not covered with the NF CSDRC. Scale bar, 5 cm. The (e) photo and (f) temperature variation of the inside of tents made of fabric and NF CSDRC. Scale bar, 15 cm.

ordinary tent, the CA NF CSDRC could lower 4.2 °C under ~850 W m^{-2} of solar radiation (Fig. 5f). From the above case, this flexible NF CSDRC has a wide range of applications as a promising passive cooling material and simultaneously exhibits aesthetic performance.

Conclusions

In summary, we developed a CA NF CSDRC, successfully realizing daytime cooling temperature below the ambient temperature and satisfying aesthetical appeal simultaneously. In addition to the selective reflection of the desired visible color, the CA NF CSDRC with 99% ultra-high NIR reflectance maximizes reflect sunlight and 95% MIR emittance efficiently dissipates radiative heat. The cooling measurement confirms that the CA NF CSDRC attains a maximum 3.2 °C cooler than ambient temperature and the net radiative cooling power ≈40 W m^{-2} under a solar intensity of 700 W m^{-2}. Moreover, the NF CSDRC possesses excellent flexibility (0.02 mN cm, below the printing paper of 63.05 mN cm and cotton cloth of 1.33 mN cm) and deformability, which can be applied to distinct scenarios in life such as tents, vehicles and textiles. Our work provides novel design and manufacturing ideas for achieving colored subambient daytime radiative coolers.

Experimental section

Materials and reagents

The CA and acetone were purchased from Sinopharm Chemical Reagent Co., Ltd (Shanghai, China). *N*,*N*-Dimethylformamide (DMF) was provided by Titan Technology Co., Ltd (Shanghai, China). Fe_2O_3 inorganic pigment (30 nm, 99.5%) was supported by Shanghai Ziyi Reagent Factory (Shanghai, China). Reactive dyes (Anozol pink, yellow and blue) were supplied by Annuoqi Fine Chemical Co., Ltd (Shandong, China).

Fabrication of CA NF CSDRC

CA NF CSDRC is fabricated as follows: CA powders were dissolved in a mixture solvent of acetone/DMF (2 : 1, w/w) to prepare the uniform CA solution (15 wt%) by stirring continuously for 2 h at ambient temperature. Afterward, nano Fe_2O_3 pigments and reactive dyes were added to the CA solution to prepare a colorful electrospinning solution. The colored CA solution was loaded into a syringe with an 18-gauge blunt tip needle. Then, the CA NF CSDRC was prepared by electrospinning technology. During the electrospinning process, the spinning parameters were as follows: voltage 20 kV, collecting distance 15 cm and propulsion speed 0.030 mm min^{-1}. The spinning conditions were room temperature and a relative humidity of 35%. The colored CA film is fabricated through drop-casting colored CA solution on the glass sheet and air drying in a fume hood.

Characterization

The morphology of the samples was observed utilizing a scanning electron microscope (JSM-7500F, JEOL, Japan) at a voltage of 5 kV after sputtering with gold for 90 s to enhance its electrical conductibility. The diameter of the CA nanofiber was calculated using ImageJ software (NIH, USA) and 200 nanofibers were measured to analyze the average fiber diameter. The thickness of the sample was measured by a thickness tester (CH-12.7-STSX, Shanghai Liuling Instrument Factory, China). The sample stiffness was measured by using an automatic fabric stiffener (LLY-01, China) according to GB/T 18318.1-2009. The size of the fabric was (25 ± 1) mm × (250 ± 1) mm. The flexural rigidity, G, was concluded from the equation[49]

$$G = m \times C^3 \times 10^{-3} \quad (1)$$

where G is the flexural rigidity (mN cm), m is the gram weight of the sample (g m^{-2}) and C is the bending length (cm), which is half of the overhang length.

The color characteristic of CSDRC is measured by a color measurement spectrophotometer (Datacolor 850, Datacolor Trading Co., Ltd, USA) using D65 standard illuminant. The color is calculated by the reflectivity spectra of the samples and the spectral intensity of the D65 light. Spectrum to color conversion is then performed by using the CIE model. Using the spectral reflected intensity and the color matching functions, the parameters X, Y, and Z, which correspond to coordinates in the CIE color space, can be calculated:[35,38,41]

$$X = 100\frac{\int_{380\text{nm}}^{780\text{nm}} I_{D65}(\lambda)R(0,\lambda)\bar{x}(\lambda)\mathrm{d}\lambda}{\int_{380\text{nm}}^{780\text{nm}} I_{D65}(\lambda)\bar{y}(\lambda)\mathrm{d}\lambda} \quad (2)$$

$$Y = 100\frac{\int_{380\text{nm}}^{780\text{nm}} I_{D65}(\lambda)R(0,\lambda)\bar{y}(\lambda)\mathrm{d}\lambda}{\int_{380\text{nm}}^{780\text{nm}} I_{D65}(\lambda)\bar{y}(\lambda)\mathrm{d}\lambda} \quad (3)$$

$$Z = 100\frac{\int_{380\text{nm}}^{780\text{nm}} I_{D65}(\lambda)R(0,\lambda)\bar{z}(\lambda)\mathrm{d}\lambda}{\int_{380\text{nm}}^{780\text{nm}} I_{D65}(\lambda)\bar{y}(\lambda)\mathrm{d}\lambda} \quad (4)$$

Normalized x, y, and z parameters can be used to identify the color in the chromaticity diagram. They are calculated as

$$x = \frac{X}{X+Y+Z} \quad (5)$$

$$y = \frac{Y}{X+Y+Z} \quad (6)$$

$$z = \frac{Z}{X+Y+Z} \quad (7)$$

The L, a, b parameters of the color is calculated by the Lab-*XYZ* color space conversion

$$L = 116\,f(Y/Y_n) - 16 \quad (8)$$

$$a = 500[f(X/X_n) - f(Y/Y_n)] \quad (9)$$

$$b = 200[f(Y/Y_n) - f(Z/Z_n)] \quad (10)$$

where X_n, Y_n, and Z_n are the tristimulus values of the white object, and

$$f(s) = s^{1/3} \text{ if } s > (24/116)^3 \quad (11)$$

$$f(s) = (841/108)s + 16/116 \text{ if } s \leq (24/116)^3 \qquad (12)$$

The solar spectrum (0.3–2.5 μm) reflectance was measured using a UV-vis-NIR spectrometer (UV3600, Shimadzu Instruments Co., Ltd, Japan, with a standard barium sulfate whiteboard for the calibration) with a diffuse integrating sphere. The MIR (3–16 um) reflectance and transmittance were measured using a Fourier transform infrared spectrometer (FTIR, Nicolet 8700, Thermo Fisher, USA) accompanied by a diffuse gold integrating sphere (PIKE Technologies).

Thermal property measurements

To evaluate the cooling capability of samples, the outdoor daytime radiative cooling test was carried out on the balcony of the building at Donghua University, Shanghai, China. The self-designed device was adopted to measure the real-time temperature under direct sunlight radiation to verify the daytime cooling performance of NF CSDRC. The self-designed testing device was composed of a thermocouple (WZPT, Songdao, China), a cooling test box, a solar radiometer and hygrometer (Tiannuo Huanneng Instrument Co., Ltd, Jinzhou, China), a temperature recorder with feedback-controlled (TP700, Tuopurui Electronics Co., Ltd, Shenzhen, China). The cooling test box was utilized to prevent heat loss in the form of thermal conduction and convection. The solar radiometer with an accuracy of ±5% was to record the solar irradiation outside the box, and a hygrometer with an accuracy of ±0.1% RH was to measure the relative air humidity. The thermocouples (with a precision of ±0.1 °C) connected with the temperature recorder have recorded the sample and ambient temperature. Moreover, the temperature recorder can use the feedback-controlled system to heat the sample to maintain the sample at ambient temperature and accurately assess the cooling power.

Conflicts of interest

There are no conflicts to declare.

Acknowledgements

This work was partly supported by the grants (51973027 and 52202218) from the National Natural Science Foundation of China, the Fundamental Research Funds for the Central Universities (2232020A-08), the Chang Jiang Scholars Program and the Innovation Program of Shanghai Municipal Education Commission (2019-01-07-00-03-E00023) to Prof. Xiaohong Qin, DHU Distinguished Young Professor Program, the Shanghai Committee of Science and Technology (no. 22ZR1401000) and the Shanghai Pujiang Program (21PJ1400200) to Prof. Dongxiao Ji.

References

1 Heating and Cooling US Department of Energy, .
2 U.S. Energy Information Administration, 2020, **https://www.eia.gov/outlooks/aeo/**.
3 R. Hu, Y. Liu, S. Shin, S. Huang, X. Ren, W. Shu, J. Cheng, G. Tao, W. Xu, R. Chen and X. Luo, *Adv. Energy Mater.*, 2020, **10**, 1903921.
4 Z. Li, Q. Chen, Y. Song, B. Zhu and J. Zhu, *Adv. Mater. Technol.*, 2020, **5**, 1901007.
5 Y. Peng and Y. Cui, *Joule*, 2020, **4**, 724–742.
6 D. Zhao, A. Aili, Y. Zhai, S. Xu, G. Tan, X. Yin and R. Yang, *Appl. Phys. Rev.*, 2019, **6**, 021306.
7 A. Addeo, L. Nicolais, G. Romeo, B. Bartoli, B. Coluzzi and V. Silvestrini, *Sol. Energy*, 1980, **24**, 93–98.
8 S. C. B. Bartoli, B. Coluzzi, V. Cuomo, V. Silvestrini and G. Troise, *Appl. Energy*, 1977, **3**, 267–286.
9 M. M. P. Berdahl and F. Sakkal, Lawrence Berkeley Laboratory, *Int. J. Heat Mass Transfer*, 1983, **26**, 871–880.
10 C. G. Granqvist and A. Hjortsberg, *J. Appl. Phys.*, 1981, **52**, 4205–4220.
11 H. Zhong, Y. Li, P. Zhang, S. Gao, B. Liu, Y. Wang, T. Meng, Y. Zhou, H. Hou, C. Xue, Y. Zhao and Z. Wang, *ACS Nano*, 2021, **15**, 10076–10083.
12 P. Li, A. Wang, J. Fan, Q. Kang, P. Jiang, H. Bao and X. Huang, *Adv. Funct. Mater.*, 2021, **32**, 2109542.
13 B. Ko, D. Lee, T. Badloe and J. Rho, *Energies*, 2018, **12**, 89.
14 M. Kim, D. Lee, S. Son, Y. Yang, H. Lee and J. Rho, *Adv. Opt. Mater.*, 2021, **9**, 2002226.
15 D. Chae, H. Lim, S. So, S. Son, S. Ju, W. Kim, J. Rho and H. Lee, *ACS Appl. Mater. Interfaces*, 2021, **13**, 21119–21126.
16 D. Chae, M. Kim, H. Lim, D. Lee, S. Son, J. Ha, J. Rho and H. Lee, *Opt. Mater.*, 2022, **128**, 112273.
17 C. Lin, Y. Li, C. Chi, Y. S. Kwon, J. Huang, Z. Wu, J. Zheng, G. Liu, C. Y. Tso, C. Y. H. Chao and B. Huang, *Adv. Mater.*, 2022, **34**, e2109350.
18 D. Chae, M. Kim, P. H. Jung, S. Son, J. Seo, Y. Liu, B. J. Lee and H. Lee, *ACS Appl. Mater. Interfaces*, 2020, **12**, 8073–8081.
19 E. Rephaeli, A. Raman and S. Fan, *Nano Lett.*, 2013, **13**, 1457–1461.
20 K. Yao, H. Ma, M. Huang, H. Zhao, J. Zhao, Y. Li, S. Dou and Y. Zhan, *ACS Appl. Nano Mater.*, 2019, **2**, 5512–5519.
21 Y. M. Yao Zhai, S. N. David, D. Zhao, R. Lou, G. Tan, R. Yang and X. Yin, *Science*, 2017, **355**, 1062–1066.
22 A. P. Raman, M. A. Anoma, L. Zhu, E. Rephaeli and S. Fan, *Nature*, 2014, **515**, 540–544.
23 Y. L. Jinlei Li, W. Li, N. Xu, B. Zhu, Z. Wu, X. Wang, S. Fan, M. Wang and J. Zhu, *Sci. Adv.*, 2022, **8**, eabj9756.
24 A. A. Babar, D. Miao, N. Ali, J. Zhao, X. Wang, J. Yu and B. Ding, *ACS Appl. Mater. Interfaces*, 2018, **10**, 22866–22875.
25 Y. F. Jyotirmoy Mandal, A. C. Overvig, M. Jia, K. Sun, N. N. Shi, H. Zhou, X. Xiao, N. Yu and Y. Yang, *Science*, 2018, **362**, 315–319.
26 J. Mandal, M. Jia, A. Overvig, Y. Fu, E. Che, N. Yu and Y. Yang, *Joule*, 2019, **3**, 3088–3099.
27 Y. Z. Tian Li, S. He, W. Gan, Z. Wei, M. Heidarinejad, D. Dalgo, R. Mi, X. Zhao, J. Song, J. Dai, C. Chen, A. Aili, A. Vellore, A. Martini, R. Yang, J. Srebric, X. Yin and L. Hu, *Science*, 2019, **364**, 760–763.
28 D. Li, X. Liu, W. Li, Z. Lin, B. Zhu, Z. Li, J. Li, B. Li, S. Fan, J. Xie and J. Zhu, *Nat. Nanotechnol.*, 2020, **16**, 153.

29 S. Atiganyanun, J. B. Plumley, S. J. Han, K. Hsu, J. Cytrynbaum, T. L. Peng, S. M. Han and S. E. Han, *ACS Photonics*, 2018, **5**, 1181–1187.
30 H. Kang, Y. Qiao, Y. Li, W. Qin and X. Wu, *Ind. Eng. Chem. Res.*, 2020, **59**, 15226–15232.
31 X. Li, J. Peoples, P. Yao and X. Ruan, *ACS Appl. Mater. Interfaces*, 2021, **13**, 21733–21739.
32 Y. Tang, G. Liang, J. Chen, S. Yu, Z. Li, L. Rao and B. Yu, *Opt. Express*, 2017, **25**, 20598–20611.
33 Y. Tang, Z. Li, G. Liang, Z. Li, J. Li and B. Yu, *Opt. Express*, 2018, **26**, 27716–27725.
34 X. Li, Y. Yang, Z. Quan, L. Wang, D. Ji, F. Li, X. Qin, J. Yu and S. Ramakrishna, *Chem. Eng. J.*, 2022, **430**, 133093.
35 W. Li, Y. Shi, Z. Chen and S. Fan, *Nat. Commun.*, 2018, **9**, 4240.
36 G. J. Lee, Y. J. Kim, H. M. Kim, Y. J. Yoo and Y. M. Song, *Adv. Opt. Mater.*, 2018, **6**, 1800707.
37 H. H. Kim, E. Im and S. Lee, *Langmuir*, 2020, **36**, 6589–6596.
38 R. A. Yalçın, E. Blandre, K. Joulain and J. Drévillon, *ACS Photonics*, 2020, **7**, 1312–1322.
39 C. Sheng, Y. An, J. Du and X. Li, *ACS Photonics*, 2019, **6**, 2545–2552.
40 D. Shu, K. Fang, X. Liu, Y. Cai, F. An, G. Qu and Y. Liang, *J. Cleaner Prod.*, 2019, **241**, 118370.
41 S. Dang, J. Xiang, H. Yao, F. Yang and H. Ye, *Energy Build.*, 2022, **259**, 111861.
42 L. Cai, Y. Peng, J. Xu, C. Zhou, C. Zhou, P. Wu, D. Lin, S. Fan and Y. Cui, *Joule*, 2019, **3**, 1478–1486.
43 B. Shan, X. Tong, W. Xiong, W. Qiu, B. Tang, R. Lu, W. Ma, Y. Luo and S. Zhang, *Dyes Pigm.*, 2015, **123**, 44–54.
44 Y.-Q. Zhang, X.-C. Wei and J.-J. Long, *J. Cleaner Prod.*, 2016, **133**, 746–756.
45 U. H. Siddiqua, M. Irfan, S. Ali, A. Sahar, M. Khalid, M. S. Mahr and J. Iqbal, *J. Mol. Struct.*, 2020, **1221**, 128753.
46 F. Shi, Q. Liu, H. Zhao, K. Fang, R. Xie, L. Song, M. Wang and W. Chen, *ACS Sustainable Chem. Eng.*, 2021, **9**, 10361–10369.
47 S. Yu, Q. Zhang, Y. Wang, Y. Lv and R. Ma, *Nano Lett.*, 2022, **22**, 4925–4932.
48 T. Wang, Y. Wu, L. Shi, X. Hu, M. Chen and L. Wu, *Nat. Commun.*, 2021, **12**, 365.
49 S. Zhong, L. Yi, J. Zhang, T. Xu, L. Xu, X. Zhang, T. Zuo and Y. Cai, *Chem. Eng. J.*, 2021, **407**, 127104.